Ames
7N-35-TM
79391

Ref 17

AIAA
P-34

NATIONAL AERONAUTICS AND SPACE ADMINISTRATION

PROPOSED JOURNAL ARTICLE

MULTIELEMENT MAPPING OF α-SiC BY SCANNING AUGER MICROSCOPY

by R. Browning
Ames Research Center
Mountain View, California 94035

and

J.L. Smialek and N.S. Jacobson
Lewis Research Center
Cleveland, Ohio 44135

RECEIVED
NASA STI FACILITY
1985 JUN 16 AM 8:55
T.I.S. LIBRARY

(NASA-TM-89624) MULTIELEMENT MAPPING OF ALPHA-SiC BY SCANNING AUGER MICROSCOPY (NASA) 34 p Avail: NTIS

N87-70440

Unclas
00/35 0079391

Prepared for

February 1986

MULTIELEMENT MAPPING OF α-SiC BY SCANNING AUGER MICROSCOPY

R. Browning*
National Aeronautics and Space Administration
Ames Research Center
Mountain View, CA 94035

and

J.L.S. Smialek and N.S. Jacobson
National Aeronautics and Space Administration
Lewis Research Center
Cleveland, Ohio 44135

E-2917

ABSTRACT

Fine second phase particles, found to be numerous in sintered α-SiC, were analyzed by scanning auger microscopy and conventional techniques. Computer controlled data acquisition, multielement CORRELATION DIAGRAMS, ~~analysis techniques~~, and a high spatial resolution of 100 nm. The Auger analysis utilized THIS enabled construction of false color ~~composition~~ maps and the detection of fine compositional details within ~~of~~ these particles. Carbon, oxide, and boron-rich particles (as BN or B_4C) predominated. BN particles, sometimes having a carbon core, ARE BELIEVED TO ~~resulted~~ from reaction between B_4C additives and nitrogen sintering atmospheres.

INTRODUCTION

Pressureless sintered α-SiC generally relies upon the addition of carbon and boron ~~on~~ or aluminum sintering aids for full densification. In the case of a prominent commercial material** these aids are known to be in the form of carbon and B_4C. Although sufficient elemental carbon and boron are active to cause densification, it has recently been verified that numerous particles of carbon and B_4C remain after processing (Refs. 1 to 5). The carbon-rich regions can be identified by standard microprobe wavelength dispersive analyses, but boron ~~identification~~ detection typically required SIMS, EELS, or scanning auger microscopy. The purpose of the present study is to characterize these

---

*Presently at Stanford University, ~~Palo Alto~~ Stanford, CA.
**Hexaloy, Carboundum Co., Niagara Falls, NY.

residual particles in two different batches of sintered SiC using high resolution scanning auger microscopy. A distinguishing feature of this study is the application of multielement mapping of compositional variations within individual particles.

EXPERIMENTAL PROCEDURE

The material used in this study is commercially available sintered α-SiC referred to as SiC-1 (vintage 1984) and SiC-2 (vintage 1977). Sintering aids of B and C were present at about the 0.5 wt % level (Ref. 1). Samples were prepared by conventional ceramographic polishing and etching in boiling Murakami's etch. Microstructural features were first characterized by routine optical microscropy, SEM, and microprobe techniques. The scanning auger microscope studies were also performed on polished and etched surfaces.

The details of the scanning auger instrument have been previously reported (Ref. 6). It is a fully computerized scanning electron microscope (SEM) and scanning auger microscope (SAM) based on a cylindrical mirror analyser (CMA) with an integral field emission source electron gun. This SEM/SAM combination is unusual in several respects important to this study. Firstly the microscope has a high spatial resolution for an auger microscope; An electron spot size of less than 100 nm was used in this work. The electron beam conditions used were 5 keV with a beam current of 3 nA and a CMA resolution of 1 percent. The spatial resolution of the auger microprobe during collection of full spectra was less than 200 nm. This figure depends not only on the electron spot size but also on the mechanical and electronic stabilities over the collection time for a spectrum. The resolution during multielement analysis however was basically the same as the spot size (100 nm) due to the fast aquisition time of this operational mode.

The second important difference between this and conventional auger microscopes is the computer controlled data collection and reduction

techniques used for microstructural analysis. For example this design allows for simultaneous multielement spectral analyses of each pixel by stepping the beam, point by point, over the area to be imaged. The data is then retrieved and presented in the form of scatter diagrams. These diagrams represent the multielement auger intensities of each pixel as a single data point in a specified composition space. Windows are defined over regions in composition space to correspond to certain phases or elements of interest. Each window is assigned a color and the final image is then constructed as a false color composition map of the region.

The obvious advantage of such a technique is the display of correlations of elements in real space, such as specific phases, to form a multielement composition map. However other advantages accrue from this technique such as improved sampling statistics and limits of detection, as well as reduced sensitivity to problems arising from beam current drift, image drift, and topographic variations. The development and use of this technique was explained in more detail in prior publications (Refs. 6 and 7) and it will be illustrated later.

RESULTS

General Microstructure

The microstructures of polished and etched samples is shown in Fig. 1. The grain sizes were approximately 4.0±0.4 and 4.5±0.4 μm for SiC-1 and SiC-2 respectively. However many excessively large 250 μm long tabular grains were also found in SiC-2. Many dark inclusions are apparent on the order of the grain size, i.e. 1 to 5 μm. The volume fractions were estimated from image analysis ~~by point counting~~ to be 9.6±1.3 and 9.2±1.3 for SiC-1 and SiC-2, respectively. Although some of these features were undoubtedly voids, many were found to be carbon-rich particles from conventional wavelength dispersive electron microprobe x-ray maps, as shown in Fig. 2 for SiC-1. The same result was found for SiC-2

(Ref. 4). The distribution of these carbon-rich particles, the lamellar structure and their association with porosity is shown quite distinctly in the conventional SEM backscatter electron (BSE) micrographs of Fig. 3. This morphology of the carbon-rich particles, which appear dark in BSE images, is reminiscent of the "fibrous texture" found in STEM analysis of graphitic particles in the same material (Ref. 3). The tendency of some particles to penetrate grain boundaries at triple points is suggested by the cusps of the particle in Fig. 4.

Scanning Auger Microscopy (SAM)

SAM was primarily used to further characterize the composition of the dark particles in both materials. Operation in the secondary electron mode proved to be fruitful in locating regions rich in oxygen (light), ~~or~~ carbon, ~~are~~ or boron (dark). This advantage over conventional SEM resulted from operation at low voltage, (5 kV), use of clean surfaces and free from any ~~surface~~ contamination films or conductive coatings. An SEM image obtained in the auger microscope of a triple point particle is shown in Fig. 5(a). The auger spectrum from an area including the triangular inclusion showed that boron, carbon and nitrogen were present with no other elements in any significant quantity, that is greater than approximately 5 at %. However this is not to say that the entire particle was a single homogeneous phase composed of B, C, and N. On the contrary, spectra obtained from various locations within this particle revealed wide variations in the B, N, C, Si, and O intensities, Figs. 6(a) to (c). (The specific nomenclature of these spectra will become evident below.) The peak intensities varied greatly with small changes in position so that the probability of overlap during any given spectral collection was high. Furthermore no distinguishing features were prominent within the SEM image of the particle which could have served as a guide to compositional analysis of each microregion. The above considerations therefore make a detailed analysis

of this complex particle impractical by conventional treatment of the data, even with the high resolution available.

The procedure for multielement analysis by scatter diagrams and false-color imaging was then followed as a means to circumvent these complications. The E.N(E) spectrum was sampled at six energies for each point in a 32 by 32 point digital raster of the image at the highest spatial resolution of 100 nm. The energies were chosen at the auger transition peak heights and at the adjacent background level on the high energy side, e.g., for carbon at 256 and 270 eV, for boron at 156 and 175 eV, and for nitrogen at 356 and 385 eV. The background counts were subtracted from the peak intensities and normalized (divided) by the sum of two counts (Ref. 8).

Relative B, N, and C intensities are therefore obtained for each pixel and represent a single data point in three-dimensional composition space. The frequency of occurrence of specific compositions within a region can be examined by plotting each of the 1024 pixel data points in two-dimensional composition space, i.e., a scatter diagram. Various scatter diagrams for the region of Fig. 5(a) are shown in Fig. 7. B is found to be spatially anticorrelated with C, as the pixels with high B have low C and versa versa (Fig. 7(a)). The same anticorrelation exists for N and C (Fig. 7(b)). However N and B are highly correlated to each other in that regions of high N are also high in B and regions of low N are low in B (Figs. 7(a) to (c)).

The distribution of data points in the scatter diagrams can now be used to identify the major elemental associations. The primary cluster at an intermediate amount of C and zero B or N arises from ~~is for~~ the SiC matrix surrounding the particle, Fig. 7(a) and (b)). The more diffuse band, above the SiC cluster and at about a 20° negative slope to the horizontal, is for the particle, Figs. 7(a) and (b). The minor distribution at zero B (or N) and C was found by spectral analyses of these regions to be oxygen ~~analyzer~~ rich.

The windows arbitrarily set to produce the false color image of each pixel data point and ultimately the complete SAM map of Fig. 3 are shown in the scatter diagram of Fig. 7(d). Here B and N have been summed together because of their high degree of correlation. Regions of high B + N and low C are green; regions of high C and zero B + N are red; and the overlap between B + N and C is brown (Table I). Oxide regions of zero B + N and C are purple, and the overlap regions of oxide containing some B + N and C are ochre. Finally the high density region of intermediate C, representing the SiC matrix, is represented by the white background.

These windows and color assignment produced the false color image of the particle and matrix in Fig. 5(b). Basically there is a carbon-rich core, a periphery of only B + N or of overlap between B + N and C, and an O-rich corner. No standard reference is available for stochiometric boron nitride which precludes an exact analyses. But these regions are likely to consist of primarily BN based on the high degree of B, N correlation. ~~However~~ These regions always contain some C (Fig. 6(a) and (b)), although the C level varied considerably in these regions. This variation could result from extremely fine B_4C areas, overlap due to C-rich adjacent areas, surface contamination, or imperfect sputter cleaning due to topographical shadowing. For example the noisy spectrum of Fig. 6(b) was obtained with a short sampling time immediately following sputter cleaning and shows a considerably reduced C peak, due only to overlap with SiC. Many of the B, N-rich regions are estimated to have less than 10 at % of C in any form by comparison with the C peaks of the SiC and C-rich regions. Conversely, the SiC and C-rich regions are quite devoid of B or N, although the C-rich area probably contains some SiC (Figs. 6(c) and (d)).

The analysis of the spectra in Fig. 6 alone gives a vague spatial ~~definition~~ description of the particle composition. It is only by the scatter

diagram/false-color imaging technique that the picture of a carbon particle surrounded by BN and oxide becomes distinctly apparent. Other particles differed in their compositional make-up. An example of a particle with a BN core and an oxide shell is shown in the SEM/SAM images of Fig. 8. Very little carbon in any form was present in this particle.

In general the BN regions were associated with carbon, oxygen, or both. This correlation can be seen in most of the larger particles imaged in Fig. 9 by the same windows and color assignments of Figs. 7 and 8. The individual particles of Figs. 7 and 8 are labeled "A" and "B", respectively. Although the false color auger micrograph in Fig. 9(b) appears quite noisy, the inclusion signal levels are well separated from the SiC signal level. Thus even single pixel events are significant and indicate the presence of individual particles. For example the single green pixel at "C" was indeed found to be BN plus some C and O from spectra obtained on this particle. A rough estimate of the total amount of boron present as BN particles was made with the assumptions that the B + N regions were 100 percent BN and the overlap regions were 50 percent BN. This value was 0.2 atomic percent boron, with lower and upper bounds of 0.~~01~~ 0.1 and 0.~~05~~ 0.5. This is compared to a value of 1.6 at % (0.43 wt %) believed to be the bulk content (Ref. 1). Also many particles were found to be primarily oxide (purple), as verified by individual spectra, Fig. 6(e).

The SiC-2 specimen was studied using the same microscope conditions as before. An example of a B-rich particle and corresponding scatter diagrams are shown in Figs. 10 and 11. The scatter diagrams indicate a distinct distribution of high B and C, a small number of C-rich, and no N-rich pixels. Windows were appropriately set (Table I) for high B + C (green), high C (red), overlap with SiC (ochre), and oxide, (purple) to produce the false color image

of Fig. 10(b). The particle is thus seen to be predominantly a B-rich phase with a small amount of spatial overlap with the SiC matrix at the periphery.

Based on the high B/C ratio observed in the spectra for this particle, and a semiquantitative comparison to the B and C peaks for BN, SiC, and C, the particle is concluded to be B_4C. A more quantitative determination was precluded by a known carbon surface contamination. No other elements were detected in wide energy scan spectra. Nitrogen was notably absent from the spectra and scatter diagrams.

At low magnification a large carbon particle was identified and numerous small particles of B_4C, C, and oxide, Fig. 12. The B_4C particles were less often associated with C or oxide than were the BN particle in SiC-1. The particle of Fig. ~~10~~ 12, ~~leveled~~ labeled "D", is typical in this respect. The amount of overall B in the image of Fig. 12 was estimated to be 0.4 at %.

DISCUSSION

The present study has characterized some of the compositional details of second phase particles found to be quite common in sintered α-SiC. Some of those particles were predominantly oxide or carbon in both materials. However the boron-rich particles in SiC-1 were BN or BN surrounding a carbon core, whereas the boron-rich particles in SiC-2 were B_4C and never exhibited a carbon core.

B_4C and free carbon are known additives in this material (refs. 1 and 9) so it is not surprising to find B_4C and C particles in SiC-2. The observation of carbon and B_4C particles is in agreement with a combined SIMS, SAM, EELS study ~~of polished sections~~ of the same material (Ref. 1). Another SAM study also found regions of high B or C content to be associated with porosity in fracture sections (Ref. 2). This is consistent with the porosity typically found to be associated with dark particles in BSE/SEM (Fig. 3).

The BN particles in SiC-1 were more puzzling until it was learned that Hexoloy can be prepared either by sintering in a nitrogen atmosphere which converts the B_4C additive to BN or in an argon atmosphere (Ref. 9). We therefore believe that SiC-1 was sintered in nitrogen and SiC-2 was sintered in argon. The conversion of boron carbide to boron nitride is expected from thermodynamics:

$$\frac{1}{2} B_4C + N_2 = 2\ BN + \frac{1}{2} C \qquad \Delta G_{2100\ ^\circ C} = \underline{-12.6}\ \text{kcal/mole} \qquad (1)$$

The false color composition maps of Fig. 5(b) is suggestive of a BN shell around a carbon core; both being reaction products according to EQN. 1 ~~(Ref. 1)~~. The particle in Fig. 8 would then be fully reacted and have released its carbon to the matrix.

The association of B-rich particles with oxide is not commonly observed but appeared frequently in this study. Some of this oxide may be an artefact of etching in boiling Murakami solution, however this could not explain the many regions consisting entirely of oxide, devoid of any boron. The majority of oxygen-rich areas found in this study are therefore believed to originate from the ~~be caused~~ ~~by~~ residual oxide films on submicron SiC powder particles and by partial oxidation of B-rich phases during sintering.

CONCLUSIONS

The relatively recent technique of scatter diagrams/false color imaging by scanning auger microscopy has been successfully applied to the study of small 2 to 5 μm particles in sintered SiC. Combined with the high spatial resolution (100 nm) of the microscope, this technique also identified compositional details <u>within</u> particles. For example BN shells around C, oxide shells around BN, and the lack of any shells in the B_4C particles were clearly evident. The unexpected occurrence of BN particles in SiC was presumed to result from reaction of B_4C additives with an N_2 atmosphere.

This data acquisition and reduction technique was well suited to this particular study using SAM. It is expected to be advantageous for other scanning electron optical instruments where digital computer control and compositional analysis are possible, e.g., SEM and STEM.

REFERENCES

1. R.F. Davis, et al., "Microanalytical and Microstructural Analyses of Boron and Aluminum Regions in Sintered Alpha Silicon Carbide," in Scanning Electron Microscopy III, SEM Inc., pp. 1161-1167 (1984).

2. Robert Sherman, "Auger Analysis of Hot-Pressed and Sintered Silicon Carbide," J. Am. Ceram. Soc., 68 [1] C-7-C-10 (1985).

3. N.J. Tighe, pp. 127-130 in Microbeam Analysis - 1984, edited by A.D. Romig and J.I. Goldstein, San Francisco Press, San Francisco, 1984.

4. N.S. Jacobson, J.L. Smialek, "Hot Corrosion of α-SiC," J. Am. Ceram. Soc., 68, 431-439 (1986).

5. R. Hamminger, G. Grathwohl, F. Thummler, "Microanalytical Investigation of Sintered SiC, Part I," J. Mater. Sci., 18 353-364 (1983).

6. R. Browning, "Ratioed Scatter Diagrams. An Erotetic Method for Phase Identification on Complex Surfaces Using Scanning Auger Microscopy," J. Vac. Sci. Technol., A2 [4] pp. 1453-1456 (1984).

7. R. Browning, "New Methods for Image Collection and Analysis in Scanning Auger Microscopy," J. Vac. Sci. Technol., in press.

8. M. Prutton, L.A. Larson, H. Poppa, "_____," J. Appl. Phys., 54 pp. 374- (1983).

9. M. Srinivasen, Sohio Engineering Products Co., Niagara Falls, N.Y., private communication, 1985.

?

TABLE I. - KEY FOR FALSE-COLOR IMAGE MAPPING

Color	SiC-1	SiC-2
Green	BN	B_4C
Brown	BN + C overlap	—
Red	C	C
Ochre	BN + oxide overlap	B_4C + SiC overlap
Purple	Oxide	Oxide

FIGURE CAPTIONS

Fig 1. (a) SEM micrograph of a boron rich inclusion in SiC-84. (b) False color Auger image of the area corresponding to (a).

Fig 2. (a) to (e) Auger spectra from regions in SiC-84. (f) Auger spectrum from a boron rich inclusion in SiC-77.

Fig 3. Scatter diagrams from the multispectral Auger image defining fig 1b. (a) The correlation of boron and carbon. (b) the correlation of nitrogen and carbon. (c) the correlation of boron and nitrogen. (d) The correlation of boron plus nitrogen and carbon showing the signal partioning for the false color image fig 1b.

Fig 4. (a) SEM micrograph of a boron rich inclusion in SiC-84. (b) False color Auger image of the region corresponding to (a).

Fig 5. (a) SEM micrograph of a general area of SiC-84. (b) False color Auger image of the region corresponding to (a).

Fig 6. (a) SEM micrograph of a general area of SiC-77. (b) False color Auger image of the region corresponding to (a).

Fig 7. (a) SEM micrograph of a boron rich inclusion in SiC-77. (b) False color Auger image corresponding to the region in (a).

Fig 8. Scatter digrams from the multispectra Auger image defining fig 7b. (a) The correlation of boron and carbon. (b)

The correlation of nitrogen and carbon.

Fig 1

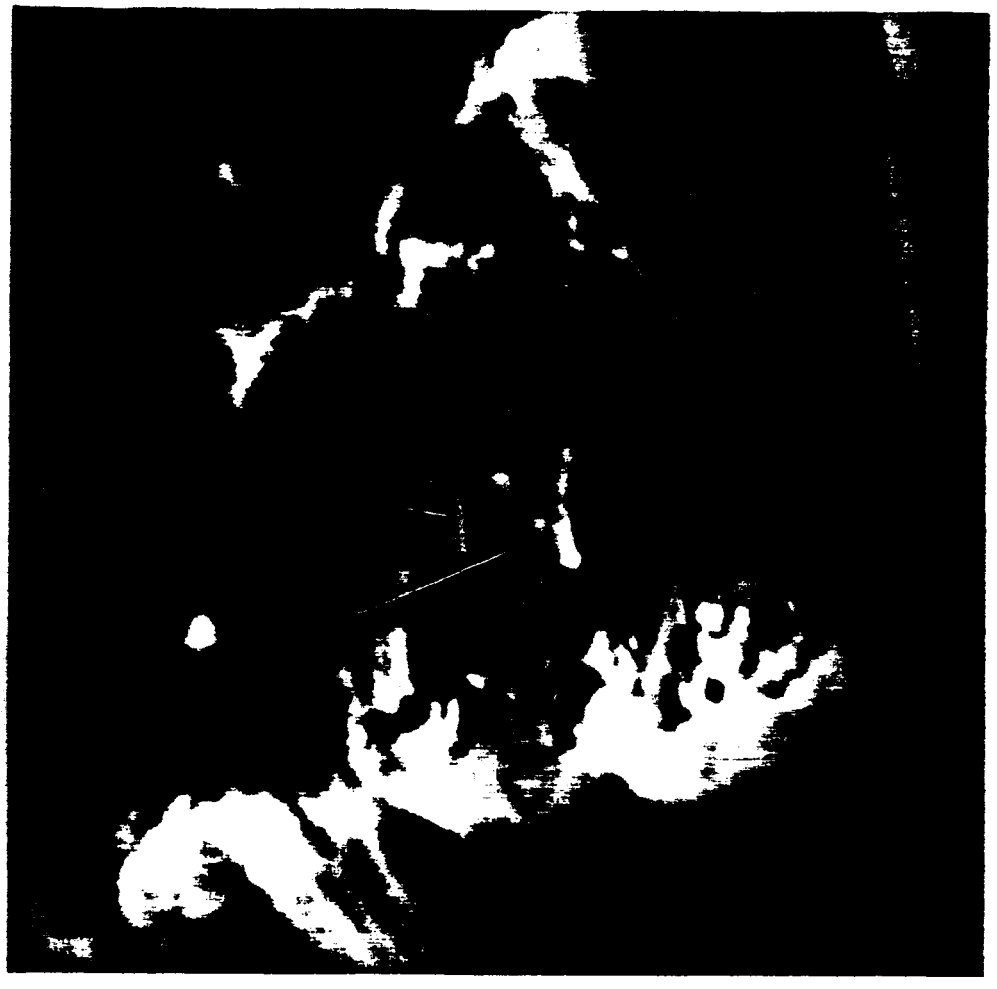

2μ

(a)

(b)

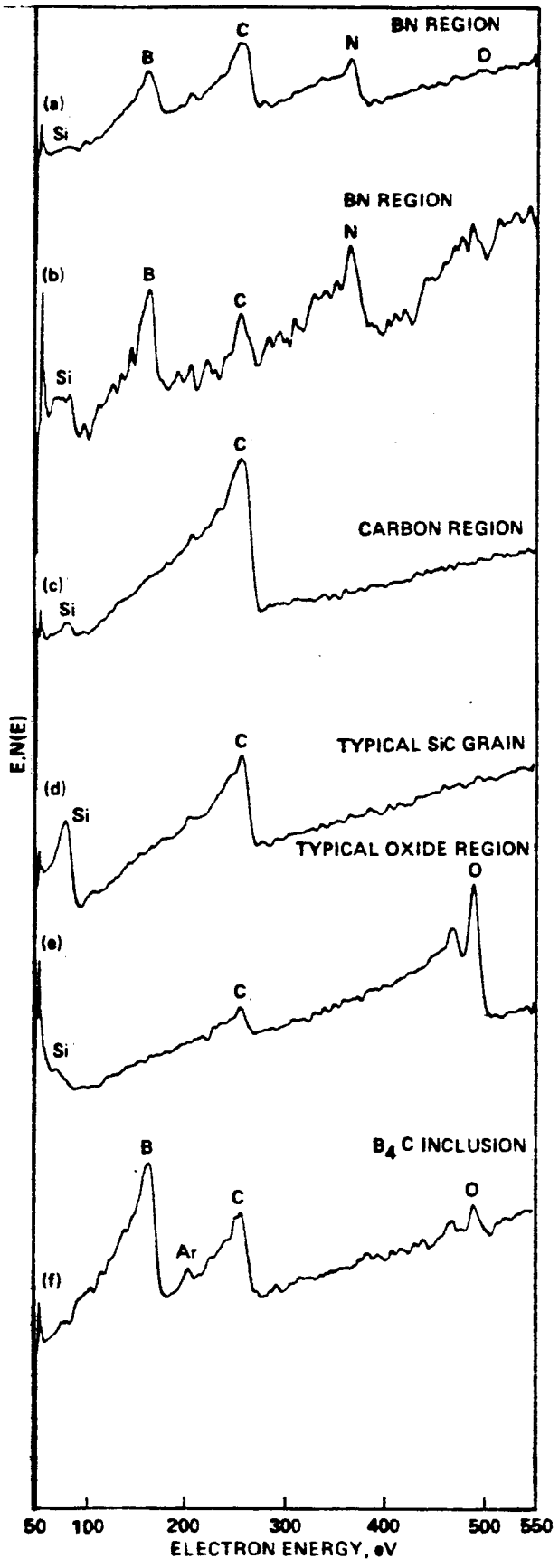
BN REGION
B
C
N
O
(a)
Si
BN REGION
N
(b)
B
C
Si
C
CARBON REGION
(c)
Si
E.N(E)
C
TYPICAL SiC GRAIN
(d)
Si
TYPICAL OXIDE REGION
O
(e)
C
Si
B
B_4C INCLUSION
C
O
Ar
(f)
50
100
200
300
400
500
550
ELECTRON ENERGY, eV

FIG 2

FIG 3

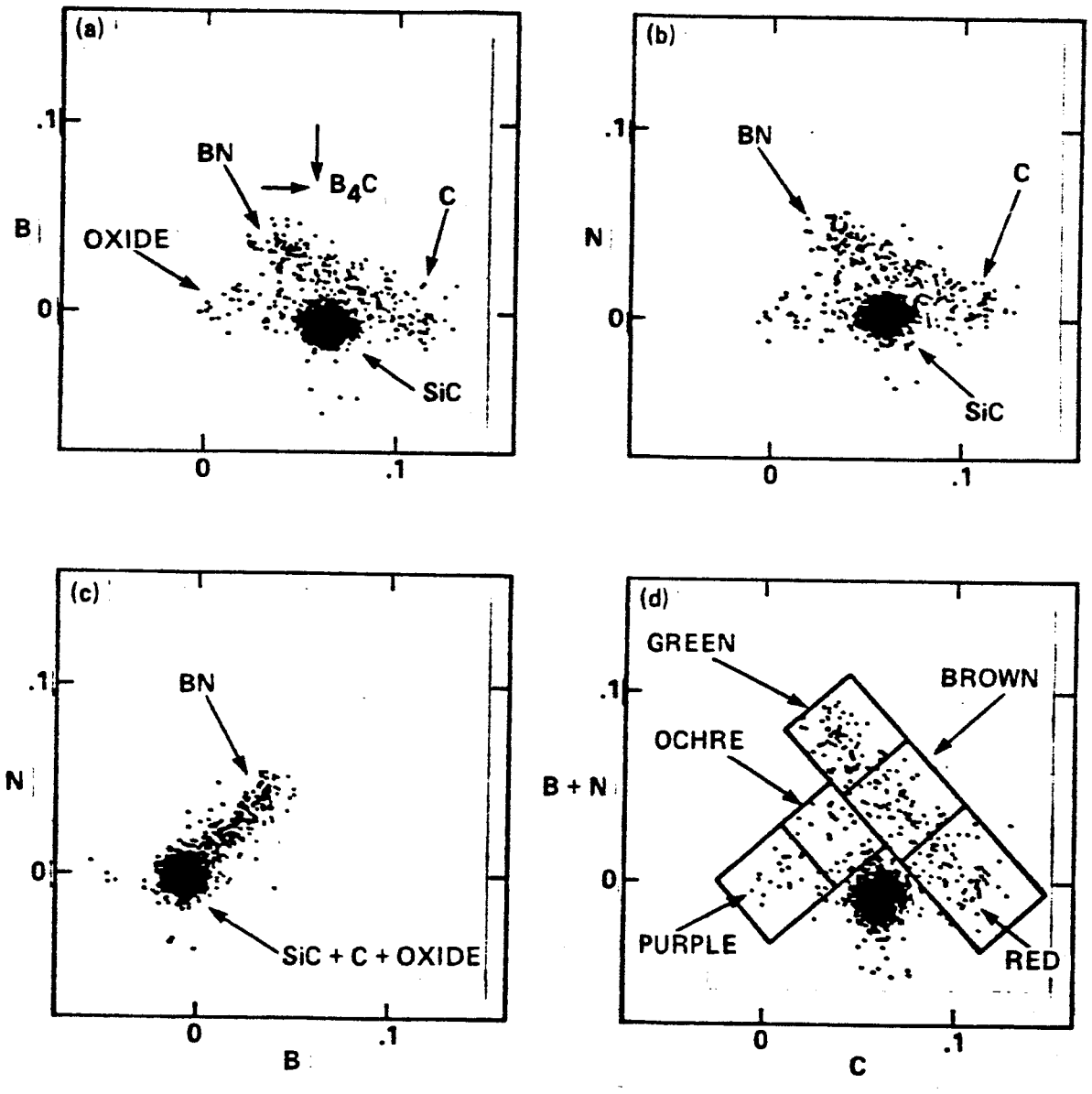

NORMALIZED AUGER INTENSITIES

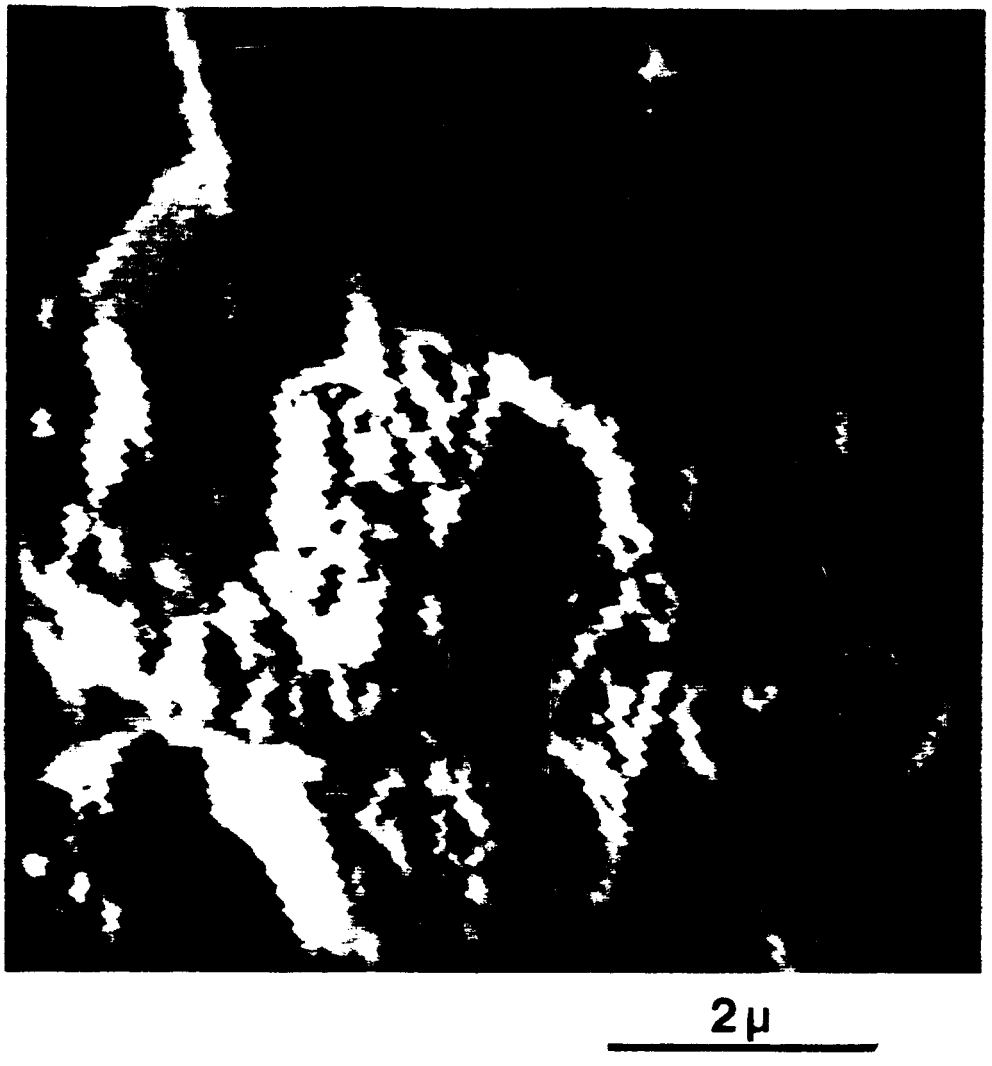

Fig 4

(a)

(b)

FIG 5

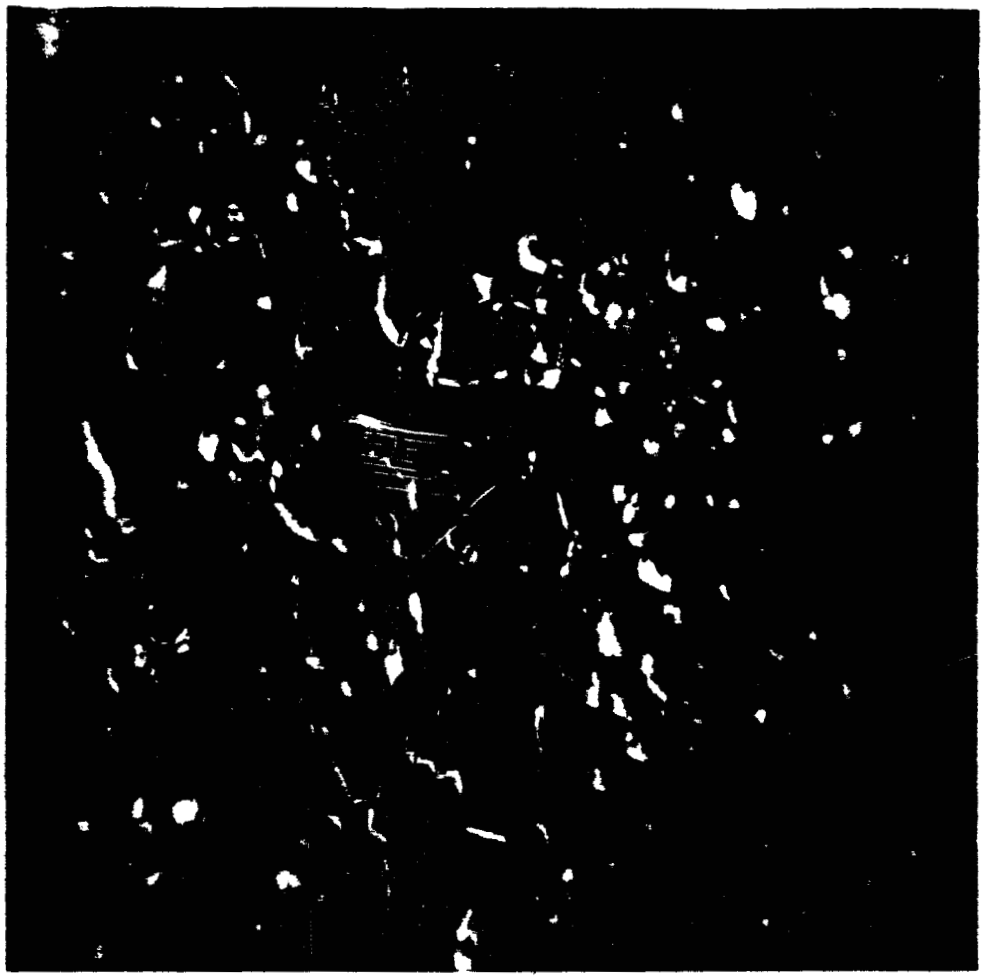

50μ

(a)

(b)

Fig 6

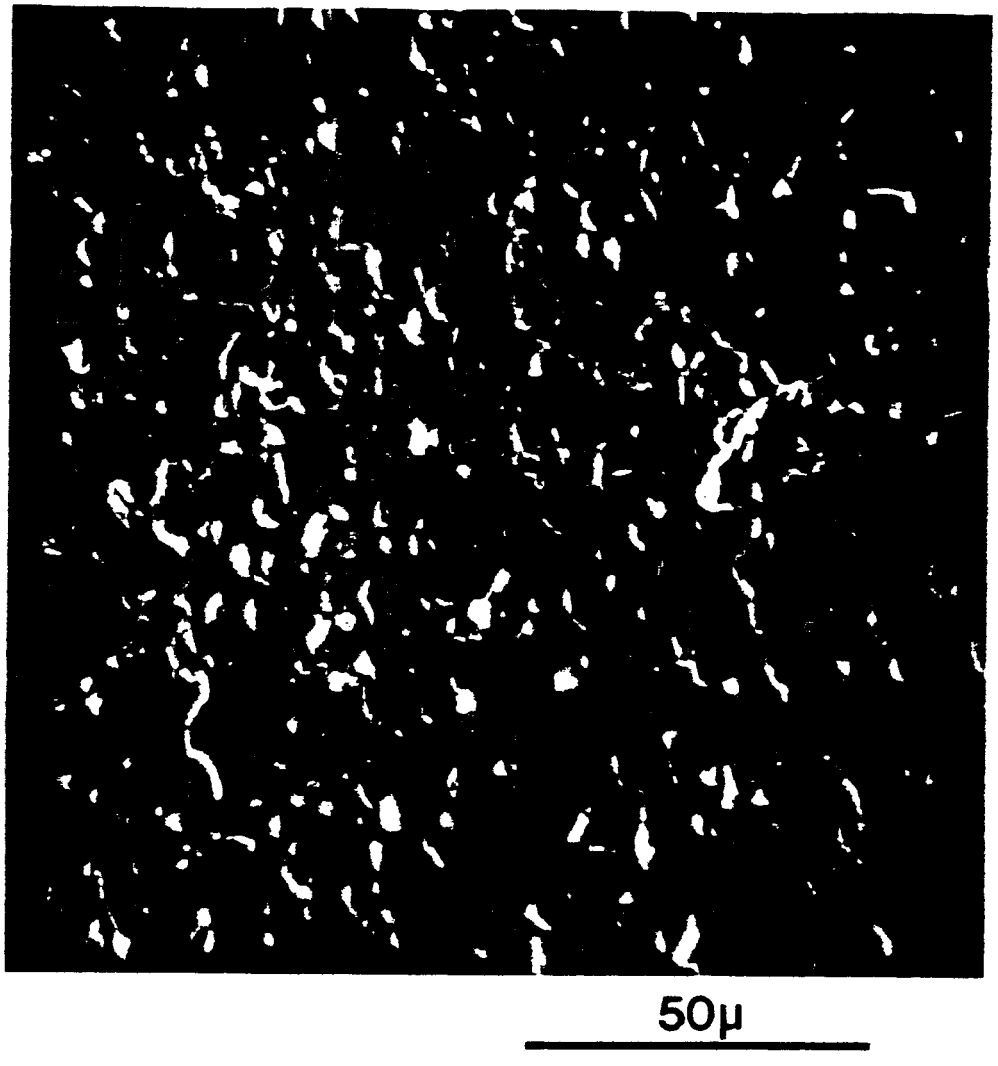

(a)

(b)

FIG 8.

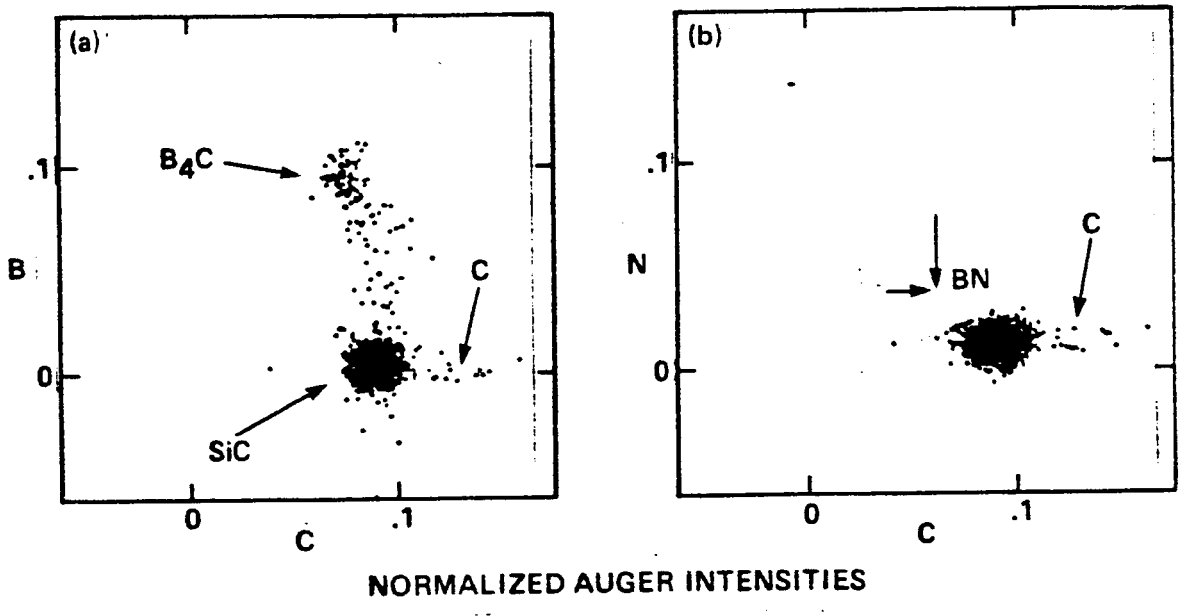
(a)
.1
B
0
B_4C
C
SiC
0
C
.1
(b)
.1
N
0
BN
C
0
C
.1
NORMALIZED AUGER INTENSITIES

Ref 18

NATIONAL AERONAUTICS AND SPACE ADMINISTRATION

PROPOSED JOURNAL ARTICLE

SCANNING AUGER MICROSCOPY OF CORRODED SiC

by R. Browning, J. Smialek, and N. Jacobson

Lewis Research Center
Cleveland, Ohio 44135

Prepared for

Jrl. Materials Science Letters

February 1986

SCANNING AUGER MICROSCOPY OF CORRODED SiC

by

R. Browning, J. Smialek, and N. Jacobson
National Aeronautics and Space Administration
Lewis Research Center
Cleveland, Ohio 44135

E-2933

~~ABSTRACT~~ INTRODUCTION

Recent molten salt corrosion studies have shown that Na_2SO_4 and Na_2CO_3 films on sintered α-SiC at 1000 °C produced substantial amounts of Na_2SiO_3 and SiO_2 (Refs. 1 to 4). When these products were removed by dissolution in a 10 percent HF solution, a severely corroded SiC substrate was revealed. This corroded material contained several interesting features including pits, inclusions, and grain boundary films. The purpose of this communication is to report an Auger examination of some of these features.

One of the most interesting features was a grain boundary film which was only observed in corrosion by basic melts-Na_2CO_3/0.1 CO_2-O_2 and Na_2SO_4/air. An example is shown in Fig. 1. Some specimens contained this feature on many boundaries; other contained it on only a few boundaries. The initial observation of this film raised several interesting questions: 1) ~~It~~ Is ~~it~~ intrinsic to carbon-doped sintered SiC[1] and revealed by the corrosion process? or, 2) Is it produced by the corrosion process and does its composition provide a clue to the mechanism of this process?

The answer to the first question was found by corroding and examining a high-purity chemical vapor deposited (CVD) SiC.[2] This is shown in Fig. 2. Note that the film appears here, indicating that is it probably not intrinsic

[1]Hexaloy, (CA. 1977), Carborundum Co., Niagara Falls, NY.
[2]General Atomics Corporation.

to sintered α-SiC. This observation is consistent with that of other investigators (Refs. 5 and 6). Therefore, the film is very likely induced by the corrosion process. Compositional information on both the film and other microstructural features may aid in understanding the corrosion process.

A preliminary attempt to characterize the corroded α-SiC films by 15 kV SEM-windowless EDS found that the C/Si peak ratios for a film triple point were ~3X greater than the ratio for the SiC grains (Ref. 1). However the resolution limit of SEM-EDS techniques (~1 μm) precluded a more definitive statement regarding these 0.1 to 0.2 μm films. GB FILM?

The primary objective of the present work was to study these films and other features of the corroded SiC in more detail using a high resolution scanning Auger microscope.

Experimental Procedure

The material used in this study was 2.5x5.0x25.0 injection molded bars of SiC doped with B_4C and C and pressureless sintered.[1] As-sintered surfaces were ground ~~by 45 and~~ to 15 μm on diamond wheels. Hot corrosion was performed by first spraying the specimens with 2.5 mg/cm^2 Na_2CO_3 salt films and then exposing to 0.1 percent CO_2 in O_2 at 1000 °C for 18 hr (Ref. 1). The corrosion products were completely removed by dissolution in H_2O-10 percent HF. Surface contaminates were removed by in situ argon in bombardment after transfer to the UHV system.

The scanning Auger microscope (SAM) used in this work has been previously described (Ref. 7). This instrument has a cylindrical mirror analyzer (CMA) with an integral field emission source electron gun. The microscope is unusual in having a high spatial resolution of less than 200 nm for this class of instrument. An electron spot size of less than 100 nm was used in this work.

---

[1]Hexaloy, (CA. 1977), ~~Carborundum Co.~~ Sohio Engineering Products Corp., Niagara Falls, NY.

[2]~~General Atomics Corporation.~~ GA Technologies, San Diego, CA

The electron beam voltage used was 5 keV with a beam current of 3×10^{-8} A and a CMA resolution of 1 percent. The spatial resolution depends not only on the electron spot size but also on mechanical and electronic stabilities over the collection time.

RESULTS AND DISSCUSION

A scanning electron micrograph obtained by the Auger instrument of one typical area of the etched and ion cleaned SiC is shown in figure 3. This micrograph shows a large corrosion pit (a), SiC grains with darker grain boundaries (b), and also what appear to be films of material decorating the grain boundaries ~~na~~ (c). These films look like mortar in a course of bricks and are typical of those previously reported (Refs. 1 and 4). Also evident but darker is inclusion (d) shown to be 80 percent carbon by Auger measurements. The SEM intensity is valuable information in this micrograph. Unlike conventional SEM where the specimen surface is contaminated with H, C, and O or even an evaporated metal coating, the argon ion cleaned surface shows considerable secondary electron contrast at the 5 kV incident energy used here. The darker area (d) is typical of carbon-rich inclusions which normally show a low secondary electron coefficient (Ref. 8).

The Auger spectra for the characteristic regions of Fig. 3 are shown in Fig. 4. It is clear that the carbon and silicon contents of the bright films and the SiC grains are nearly the same, while the dark particles are quite carbon-rich. A number of determinations showed that the SiC grains produced C/Si ratios consistent to within 1 percent. Thus the composition of these regions was assumed to be stoichiometric SiC and was used as a standard against which to compare the other regions, Table I. For example, the smooth SiC grain marked (e) in Fig. 3 was found to be slightly carbon-depleted, possibly indicating a specific crystallographic fracture plane lower in carbon than average. The light grain boundary films were only slightly enriched in

carbon, C/Si = 1.2, which is equivalent to a mixture of SiC + 18 at % C. This enrichment factor was consistent for other similar films as well. The dark particle at (d) produced a C/Si ratio of 4.37, which is equivalent to carbon + 23 at % SiC. No elements other than Si, C, O, Ar, and N were found in the spectra, the detection limit being less than 5 at %.

The other important observation is that the grain boundary films are basically SiC with a slight carbon enrichment. Since these films were also found by corroding high purity CVD SiC, they are believed to be artifacts of the corrosion process. Furthermore, no indication of a grain boundary network of carbon films was found in an associated SAM mapping study of uncorroded sintered SiC samples (Ref. 9). Thus, the films do not appear to be remnants of the free-carbon additives used as sintering aids. Also, the fact that no oxygen was observed in these films ~~incidates~~ indicates that they are not corrosion products but are very likely remnants of dissolved SiC grains. However, the details of the corrosion process that would produce this carbon-rich SiC remnant film are not clear.

Thus an Auger examination of corroded α-SiC reveals some important surface compositional information. First, carbon-rich inclusions were found which were not completely oxidized, and must therefore have existed in contact with the corrosion products. This is consistent with the conclusions of the authors in a previous paper that the carbon inclusions do not play a role in Na_2CO_3 corrosion as they do in Na_2SO_4 corrosion.

Discrete carbon-rich particles have been a common observance in EMP, STEM, SAM, and SIMS studies of this material, and they are often associated with porosity and boron-rich regions (Refs. 1, 5, 6 and 9 to 11). For example, particles have been identified by SAM as carbon cores with BN shells or as B_4C completely, depending upon the use of nitrogen or argon sintering atmospheres (Ref. 9).

CONCLUSION

Morphological features of sintered SiC were examined by high resolution SAM after 1000 °C corrosion by Na_2CO_3 films and chemical removal of the corrosion products. Carbon-rich particles were found as remnants of free-carbon sintering aid additives. This verifies an earlier conclusion that carbon does not play a role in Na_2CO_3 corrosion. Features appearing to be grain boundary films only slightly enriched in carbon were not the remains of sintering aids, but were remnants of partially consumed SiC grains.

REFERENCES

1. N.S. Jacobson, and J.L. Smialek, J. Amer. Ceram. Soc., 68, (1985) p. 432.

2. N.S. Jacobson, J. Amer. Ceram. Soc., 69 (1986) p. 74.

3. N.S. Jacobson, C.A. Stearns, J.L. Smialek, Advanced Ceramic Materials, in press.

4. J.L. Smialek, N.S. Jacobson, J. Amer. Ceram, Soc., in press.

5. R. Sherman, J. Amer. Ceram, Soc., 68, (1985) C7.

6. R. Hamminger, G. Grathwohl, F. Thummler, I,II, J. Mater. Sci., 18, (1983), 353, 3154.

7. R. Browning, J. Vac. Sci, Technol., 2 (1984) 1453

8.

9. R. Browning, J.L. Smialek, N.S. Jacobson, submitted to J. Amer. Ceram, Soc.

10. R.F. Davis, et al., Scanning Electron Microscopy III (1984), 1161.

11. N.J. Tighe, Microbeam analysis (1984), 127

TABLE I. - SAM COMPOSITION OF MICROSTRUCTURAL FEATURES IN CORRODED SiC

Feature	C/Si	Region of Fig. 3
Pitted SiC grain	1.00	(f)
Smooth SiC grin	.91	(e)
Light grain boundary film	1.22	(c)
Dark inclusion	4.37	(d)

SE 3KX

Figure 1

10KX

Figure 2

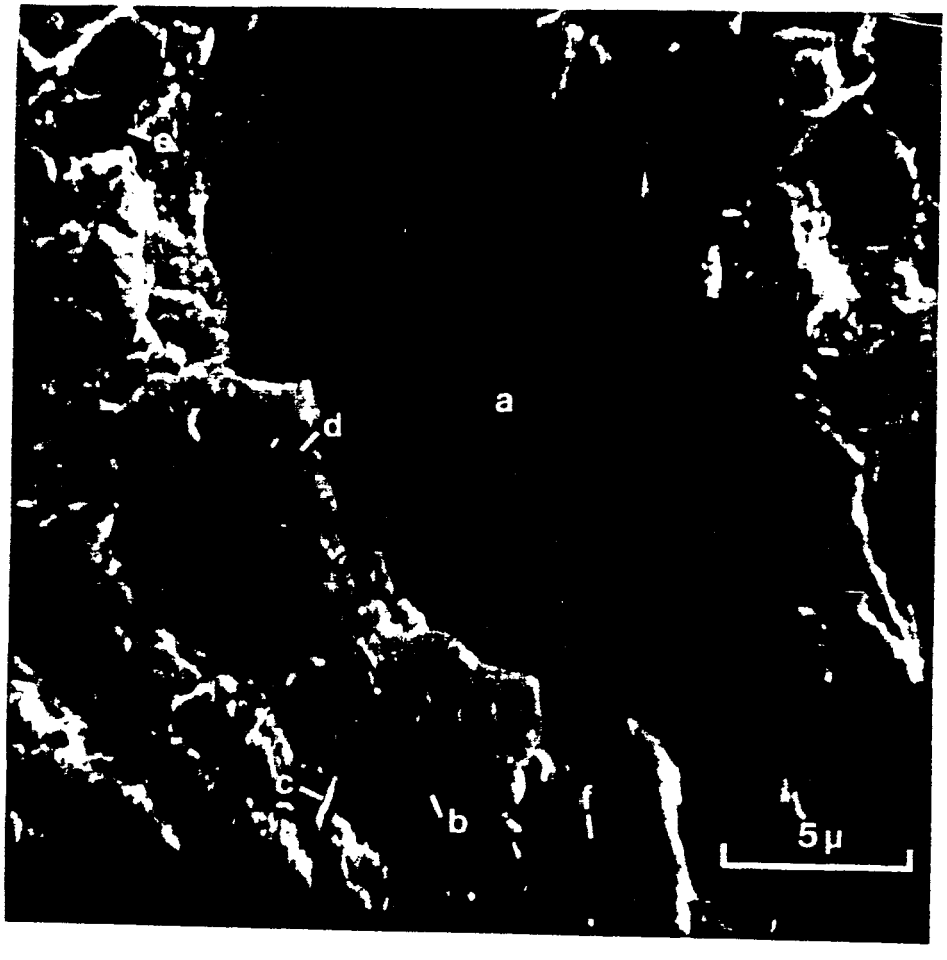

FIG 3

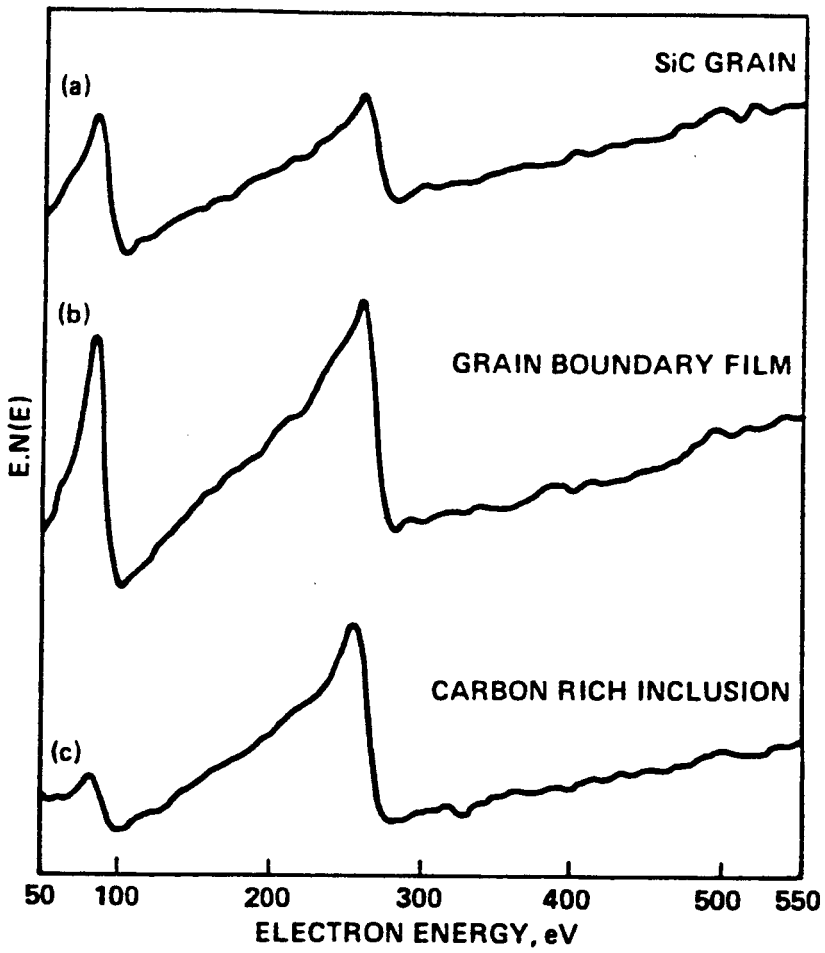

Si 92 eV
label C 272

FIG 4.